Noname manuscript No.
(will be inserted by the editor)

Influence of relative velocity on two-phase flow laminar flame structure and propagation properties

Bastien Rochette · Benedicte Cuenot · Alain Cayre · Stephane Richard

Received: date / Accepted: date

Abstract A numerical study of an one-dimensional n-heptane/air spray flame is presented. The objective is to evaluate the flame propagation speed in the case where droplets evaporate inside the reaction zone with possibly non-zero relative velocity. Numerical simulations consist in one-dimensional resolved simulations coupled to Discrete Particle Simulation for the dispersed phase. A two-step n-heptane/air chemical mechanisms is used. The effects of initial droplet diameter, overall equivalence ratio Φ_{tot} and relative velocity between gaseous and liquid phase are studied. For lean premixed cases, it is found that the laminar flame speed decreases with large initial droplet diameter and high relative velocity. On the contrary, rich premixed cases show a range of diameter for which the flame speed is enhanced compared to the purely gaseous flame.

1 Introduction

Polydisperse spray combustion occurs in a variety of combustion systems, including internal combustion engines or aviation gas turbines. The presence of a spray in a combustion chamber leads to complex phenomena spray/combustion interactions. The liquid phase may change the premixed flame propagation properties [4,14,2,10,16]. Burgoyne et al. [4] have measured one-dimensional laminar flame propagation velocities in monodisperse sprays. Their results showed that with very small droplets and very diluted sprays the propagation mechanism is that of a premixed flame. Ballal and Lefebvre [2] point out the existence of an optimum droplet size for a given fuel and overall equivalence ratio that results in an enhanced laminar flame propagation compared to perfectly premixed flame. Hayashi et al. [7] have observed the same enhancement for a wide range of overall equivalence ratio, with ethanol and n-octane mixtures of mono-sized droplets. For overall lean flames, this phenomenon was explained by a change of flame structure caused by the heterogeneous nature of the unburned mixture: the rugged and wrinkled flame front increases the flame surface. For overall rich flames, another explanation was proposed, based on an effective fuel-air ratio which accounts for the unvaporized and incompletely mixed fuel: the effective fuel would be less than the overall fuel by the amount corresponding to the unvaporized droplets and incompletely mixed fuel vapor. The resulting reacting mixture burns close to stoichiometry, leading to high flame propagation speed. The flame speed enhancement for overall rich flames has also been numerically observed in one-dimensional laminar premixed spray flames simulations [17,5,11], suggesting that 3D effects may not be the primary factor controlling this behaviour.

In all previous studies, the impact of the spray on the flame does not take into account the relative velocity between the spray and the gaseous flow. In combustion chambers, this relative velocity can be high as the air and spray injections are separated and large Stokes droplets do not

Bastien Rochette
CERFACS
42 Avenue Gaspard Coriolis 31057 Toulouse
Cedex 01, France
Tel.: ++33 (0)5 61 19 31 31
Fax: ++33 (0)5 61 19 30 30
E-mail: rochette@cerfacs.fr

immediately take the gas flow velocity. Moreover, the gas flow is often subjected to high shear, particularly in dilution area, and strong velocity gradients occur that increase the relative velocity with the droplets. Finally, turbulent velocity fluctuations may contribute to a velocity difference with the droplets.

For a better understanding of the factors controlling spray flames propagation, combustion in one-dimensional mono-disperse mists of moving droplets is studied in the current work. the objective is to characterize the effect of overall equivalence ratio, droplet size, and relative velocity on the flame structure and propagation. The paper is organized as follows. First, the numerical solver and modelling are presented in Section 2, together with the studied configuration. Then Section 3 presents results, evidencing the influence of relative velocity on the spray flame properties.

2 Numerical formulation and models

The AVBP solver is used with the Lagrangian formalism to treat the liquid phase. Droplets are considered as isolated points in space, influenced by the surrounding Eulerian gaseous flow conditions estimated at their location. In the two-way coupling approach, the liquid phase transfers mass, momentum and energy to the gas via additional source terms. A projection/interpolation procedure is needed to compute the gaseous flow conditions at the droplet location, then to exchange source terms between particles and the grid of the gas phase.

2.1 Gas phase equations

The conservation equations of mass, species, momentum and energy in the gas phase are the following:

$$\frac{\partial \rho}{\partial t} + \frac{\partial \rho u_j}{\partial x_j} = S_m^{l\to g}, \tag{1}$$

$$\frac{\partial \rho Y_k}{\partial t} + \frac{\partial \rho u_j Y_k}{\partial x_j} = \frac{\partial}{\partial x_j}\left(\rho D_k \frac{W_k}{W}\frac{\partial X_k}{\partial x_j} - \rho Y_k V_c\right) + \dot{\omega}_k + S_k^{l\to g}, \tag{2}$$

$$\frac{\partial \rho u_i}{\partial t} + \frac{\partial \rho u_i u_j}{\partial x_j} = -\frac{\partial}{\partial x_j}\left(P\delta_{ij} - \tau_{ij}\right) + S_{qdm}^{l\to g}, \tag{3}$$

$$\frac{\partial \rho E}{\partial t} + \frac{\partial \rho u_j E}{\partial x_j} = -\frac{\partial}{\partial x_j}\left(u_i\left(P\delta_{ij} - \tau_{ij}\right) + q_j\right) + \dot{\omega}_T + S_E^{l\to g}, \tag{4}$$

where ρ and u are the gaseous density and velocity. Y_k and $\dot{\omega}_k$ are the mass fractions and reaction rates of species k. X_k and W_k are the mole fraction and the atomic weight os species k. As the species diffusion coefficients D_k are expressed by the Hirschfelder and Curtiss approximation [8], a correction velocity V_c is introduced to ensure global mass conservation ($V_c = \sum_{k=1}^{N} D_k \frac{W_k}{W}\frac{\partial X_k}{\partial x_j}$). P is the pressure given by the equation of state for a perfect gas $P = \rho r T$ (r is the mixture gas constant and T the temperature), δ_{ij} is the Kronecker delta, τ_{ij} is the stress tensor: $\tau_{ij} = \mu(\frac{\partial u_i}{\partial x_j} + \frac{\partial u_j}{\partial x_i}) - \frac{2}{3}\mu\frac{\partial u_k}{\partial x_k}\delta_{ij}$, with μ the shear viscosity expressed with the power law. $\dot{\omega}_T$ is the heat release. The total heat flux q_j writes: $-\lambda\frac{\partial T}{\partial x_j} - \rho\sum_{k=1}^{N}\left(D_k\frac{W_k}{W}\frac{\partial X_k}{\partial x_j} - Y_k V_c\right)h_{s,k}$, where λ is the heat conduction coefficient of the mixture, and $h_{s,k}$ the sensible mass enthalpies of species k.

2.2 Liquid phase

The Lagrangian formalism relies on the calculation of each particle trajectory, along which source terms are applied. Transfer to the gas of mass, momentum and energy is locally estimated from a number N of droplets inside a nodal control volume ΔV. These source terms are then projected

on the corresponding grid node:

$$S_m^{l\to g} = S_k^{l\to g} = \frac{1}{\Delta V}\sum_{n=1}^{N}\psi_n\left(\overrightarrow{x}_p\right)\dot{m}_{p,n}, \tag{5}$$

$$S_{qdm,j}^{l\to g} = \frac{1}{\Delta V}\sum_{n=1}^{N}\psi_n\left(\overrightarrow{x}_p\right)\left(-m_{p,n}F_{p,n,j}^{ext} + \dot{m}_{p,n}u_{p,n,j}\right), \tag{6}$$

$$S_E^{l\to g} = \frac{1}{\Delta V}\sum_{n=1}^{N}\psi_n\left(\overrightarrow{x}_p\right)\left(-m_{p,n}\overrightarrow{F}_{p,n}^{ext}\cdot\overrightarrow{u}_{p,n} + \frac{1}{2}\dot{m}_{p,n}||\overrightarrow{u}_{p,n}||^2 - \dot{\Phi}_{p,n}\right) \tag{7}$$

where $\psi_n\left(\overrightarrow{x}_p\right)$ is the interpolation/projection function. $m_{p,n}$ is the instantaneous mass of the droplet and $\overrightarrow{u}_{p,n}$ its velocity. A film assumption [3], taking into account the change in film thickness due to Stefan low, is used by Abramzon and Sirignano [1] to modify the Sherwood number of the droplet evaporation rate $\dot{m}_{p,n}$:

$$\dot{m}_p = -Sh^*\pi d_p\rho D_F\ln\left(B_M+1\right), \tag{8}$$

$$B_M = \frac{Y_{F,surf}-Y_{F,\infty}}{1-Y_{F,surf}}, \tag{9}$$

$$Y_{F,surf} = \frac{X_{F,surf}W_F}{X_{F,surf}W_F + (1-X_{F,surf})\overline{W}_{n,F,surf}}, \tag{10}$$

$$\overline{W}_{n,F,surf} = \overline{W}_{n,F,\infty} = \frac{1-Y_{F,\infty}}{1-Y_{F,\infty}\dfrac{\overline{W}}{W_F}}\overline{W}, \tag{11}$$

$$X_{F,surf} = \frac{P_{cc}}{P}\exp\left(\frac{W_F L_v\left(T_{ref}\right)}{R}\left(\frac{1}{T_{cc}}-\frac{1}{T_{surf}}\right)\right), \tag{12}$$

where d_p is the droplet diameter. B_M is the mass transfer Spalding number, using fuel mass fraction estimated at the droplet surface with Clausius-Clapeyron equation (Eq. 12). W_F is the molar weight of the fuel and $\overline{W}_{n,F,surf}$ the molar weight of the mixture of all species other than fuel, calculated at the surface with Eq. 11. T_{cc} and P_{cc} correspond to an an arbitrary reference point on the saturation curve, R is the universal gas constant and $L_v(T_{ref}) = h_{s,F}(T_{ref} - h_{s,p}(T_{ref}))$ the latent heat at T_{ref}. An enthalpy balance applied to the droplet (Eq. 13) is done to compute the droplet temperature:

$$\frac{dc_{p,l}T_p}{dt} = \frac{1}{m_p}\left(-\dot{\Phi}_{g,n} + \dot{m}_p L_v(T_p)\right), \tag{13}$$

$\dot{\Phi}_{g,n}$ is the gaseous conductive heat flux at the droplet surface:

$$\dot{\Phi}_{g,n} = Nu^*\pi d_p\frac{\lambda}{c_p}\left(c_p(T_p)T_p - c_p(T_\infty)T_\infty\right)\frac{\ln\left(B_T+1\right)}{B_T}, \tag{14}$$

$$B_T = \left(1+B_M\right)^{1/Le_F} - 1, \tag{15}$$

where c_p is the mass constant pressure heat capacity estimated at the droplet surface temperature T_{surf} and the far field temperature T_∞. B_T is the heat transfer Spalding number, and $Le_F = \lambda/c_p\rho D_F$ the Lewis number of the fuel. As for the Sherwood number in Eq.8, the Nusselt number Nu^* used to compute $\dot{\Phi}_{g,n}$ is corrected by the Abramzon and Sirignano model [1]:

$$Sh^* = 2 + \frac{B_M}{(1+B_M)^{0.7}\ln(1+B_M)}\left(0.55Re_p^{1/2}(S_c^F)^{1/3}\right) \tag{16}$$

$$Nu^* = 2 + \frac{B_T}{(1+B_T)^{0.7}\ln(1+B_T)}\left(0.55Re_p^{1/2}Pr^{1/3}\right), \tag{17}$$

$$Re_{p,n} = \frac{\rho d_{p,n}||\overrightarrow{u}-\overrightarrow{u}_{p,n}||}{\mu}, \tag{18}$$

	A_j[cgs]	E_j[cgs]
Reaction 1	1.4×10^{11}	2.9×10^4
Reaction 2	-5.0×10^9	2.1×10^4

Table 1: Two-steps reduced chemical mechanism for n-heptane/air. Pre-exponential factor A_j and activation energies E_j are both in *cgs* units.

where P_r is the Prandtl number and Re_p the Reynolds number of the particle. Inter-droplets interactions and gravity being neglected, external forces $\overrightarrow{F}^{ext}_{p,n}$ acting on the droplet are only composed of drag force:

$$\overrightarrow{F}^{ext}_{p,n} = \frac{m_p}{\tau_p}(\overrightarrow{u} - \overrightarrow{u}_p)\,, \tag{19}$$

where τ_p is the relaxation time of the particle expressed with an empirical correlation proposed by Schiller and Naumann [15]:

$$\frac{1}{\tau_p} = \frac{18\mu\left(1 + 0.15Re_p^{0.687}\right)}{\rho_p d_p^2}. \tag{20}$$

2.3 Chemistry description

In spray flames, chemistry description plays a key role, especially in post-flame region where droplets of fuel can still evaporate and oxidize. In the current work, a simplified two-step mechanism is used for premixed n-heptane/air flames, with a Pre-Exponential Adjustement (PEA) method [6] to ensure the correct laminar flame speed in rich mixtures. This two-step mechanism is based on a fast oxydation reaction, followed by a CO-CO2 equilibirum. Six species (C_7H16, O_2, CO, $H2O$, CO_2 and N_2) and two reactions are taken into account [12]:

$$2\mathrm{C_7H_{16}} + 15\mathrm{O_2} \longrightarrow 14\mathrm{CO} + 16\mathrm{H_2O} \tag{21}$$

$$\mathrm{CO} + 0.5\mathrm{O_2} \longleftrightarrow \mathrm{CO_2} \tag{22}$$

The reaction rates q_j follow an Arrhenius law:

$$q_1 = A_1 f_1(\Phi_{loc}) \left(\frac{\rho Y_{C_7H_{16}}}{W_{C_7H_{16}}}\right)^{0.6} \left(\frac{\rho Y_{O_2}}{W_{O_2}}\right)^{0.9} \exp\left(\frac{-E_{a,1}}{RT}\right) \tag{23}$$

$$q_2 = A_2 f_2(\Phi_{loc}) \left[\left(\frac{\rho Y_{CO}}{W_{CO}}\right)^{1.0} \left(\frac{\rho Y_{O_2}}{W_{O_2}}\right)^{0.5} - \frac{1}{K}\left(\frac{\rho Y_{CO_2}}{W_{CO_2}}\right)^{1.0}\right] \exp\left(\frac{-E_{a,2}}{RT}\right) \tag{24}$$

The pre-exponential constants A_j and the activation energies E_j are given in Tab. 1, and K is the equilibrium constant. To recover the correct flame speed for rich mixtures, the Pre-Exponential Adjustement (PEA) method is used [6]. This method accounts for both the fuel oxidation reaction and the CO-CO2 equilibrium. This last reaction is difficult to handle numerically since it shows a sudden change in behaviour from lean to rich combustion. Therefore, the pre-exponential factor of the second reaction varies with local equivalence ratio Φ_{loc} using a correction function $f_2(\Phi_{loc})$ to reproduce this specific behavior. Then, the pre-exponential factor of the fuel oxidation reaction is also corrected to predict correctly the laminar flame speed.

The local equivalence ratio is based on a passive scalar $Z \in [0, 1]$ [13]. Z is calculated on the principle of atoms conservation in the gas phase. To avoid Z variations due to differential diffusion, the construction of Z requires that all species laminar Schmidt numbers are equal, which is the case for the two-step chemical scheme.

$$\Phi_{loc} = \frac{1 - Z_{st}}{Z_{st}} \frac{Z}{1 - Z}, \tag{25}$$

$$Z = \frac{n - n_O}{n_F - n_O} \text{ with } n = \sum_{k=1}^{N} \alpha_{kp} \frac{W_p Y_k}{W_k}, \tag{26}$$

Case	ϕ_{tot}	Liquid/air ratio	u_{rel}	d_p (μm)
A	0.9	$\phi_g = 0.8$, $\phi_l = 0.1$	1, 30	20-80
B	0.9	$\phi_g = 0.03$, $\phi_l = 0.87$	1, 30	20-80
C	1.3	$\phi_g = 0.8$, $\phi_l = 0.5$	1, 30	20-80

Table 2: Summary of simulated cases

where n_O and n_F stand for the values of n in the oxidizer and fuel streams respectively, α_{kp} is the number of atoms of type p in species k. The two-step scheme is validated against the experimental laminar flame speed measurements provided by Kumar et al. [9] in Fig. 1. The Cantera software is used to compute flame speeds for a 1D resolved planar flame at the same operating conditions as the simulations ($T = 300K$ and $P = 101325$ Pa): results show a good agreement for the two-step reduced chemistry for equivalence ratios ranging from $\phi_g = 0.8$ to $\phi_g = 1.4$.

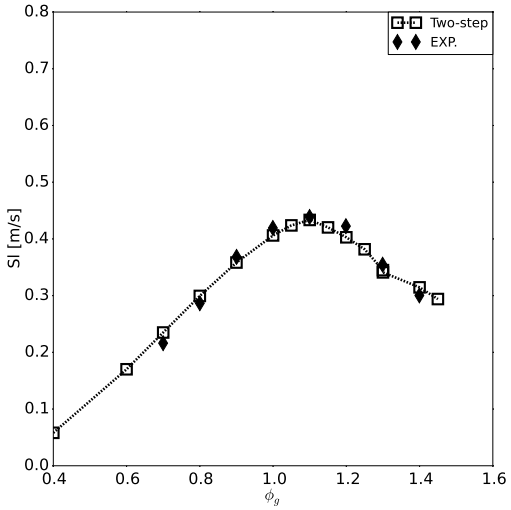

Fig. 1: *Comparison of experimental measurements [9] and two-step chemistry for laminar flame speed computed at* $T = 300K$, $P = 101325Pa$.

2.4 Configuration

The computational domain consists of a 0.02 m long cartesian one-dimensional grid, composed of 826 elements. The domain is sufficiently long to allow the liquid droplets of n-heptane to completely evaporate, and the grid is fine enough to solve the premixed inner flame structure. In such configuration, and as in purely gaseous flames, the flame can stabilize anywhere in the domain. This has a direct impact on the two-phase flame structure, as droplets may evaporate and interact with the gas flow through drag during their travel from injection to the flame. In other words, the solution of the two-phase flame depends on an additional parameter compared to gaseous flames, which is the distance from injection. This parameter however is meaningless in the case of one-dimensional flames and should not appear in the analysis. In the present work, the two-phase flame will be therefore characterized by the droplet properties just in front of the flame, i.e. at the location where they start to interact with the flame [16]. To control these properties for the proposed parametric study, droplets may either travel from injection to the flame without any interaction with the gas (i.e. exchange terms are cancelled in the simulation) or simply be injected just in front of the flame front. Table 2 summarizes the simulated cases. Two overall equivalence ratios were investigated, $\phi_{tot} = 0.9$ and $\phi_{tot} = 1.3$, with three different liquid loadings. The velocity ratio between liquid and gaseous phases is expressed as $u_{rel} = u_l/u_g$. For each liquid loading, two velocity ratios were tested

(1 and 30), with droplets of diameters ranging from $d_p = 20$ μm to 80 μm. Droplets are injected at the same temperature as the gas, $T_l = T_g = 300K$. The number of droplets is sufficiently high to ensure at least one droplet per grid element, when $d_p > 0$.

3 Results

In Section 3.1, typical spray flame structures with and without relative velocities are presented for cases A and C (cf. Tab. 2): flame structures observed in case B are similar to ones computed in case A and not shown.

3.1 Typical spray flame structures

Two n-heptane/air spray flames of cases A and C are chosen to point out the effect of relative velocity on the flame structure. The first flame is computed with droplets of initial diameter $d_p = 20$ μm and no relative velocity between droplets and gaseous flow ($u_{rel} = 1$). The second one is computed with the same droplets initial diameter $d_p = 20$ μm but with a velocity ratio $u_{rel} = 30$. Resulting temperature profiles are compared to a gaseous premixed flame solution at the same total equivalence ratio.

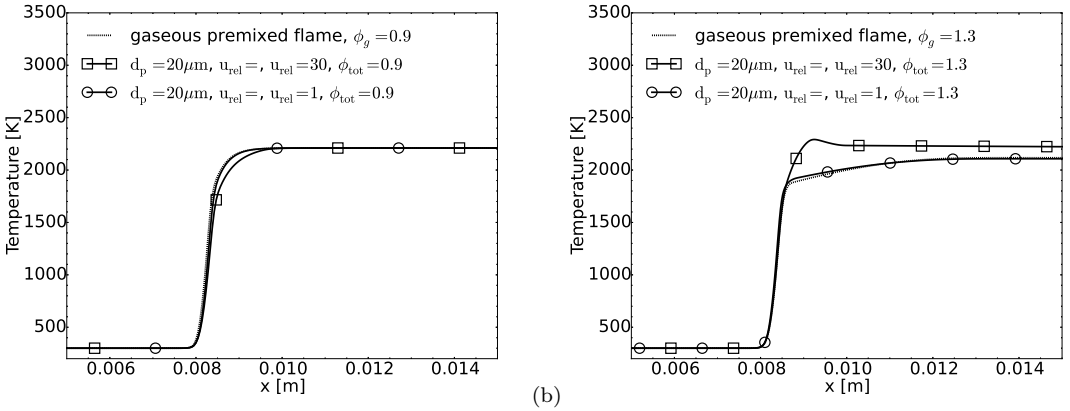

Fig. 2: *Comparison of temperature profiles for gaseous and spray flames computed with two total equivalence ratios: (a)*$\phi_{tot} = 0.9$*:* $\phi_g = 0.8, \phi_l = 0.1$ *and (b)* $\phi_{tot} = 1.3$*:* $\phi_g = 0.8, \phi_l = 0.5$*. Droplet diameter is* $d_p = 20\mu m$ *and velocity ratios are* $u_{rel} = 1$ *and* $u_{rel} = 30$*.*

Figure 2 (a) shows temperature profiles for case A (i.e lean mixture and small liquid loading), and Figs. 3 (a) and (b) the corresponding source terms for $u_{rel} = 1$ and $u_{rel} = 30$. For $u_{rel} = 1$, the spray flame structure is similar to the gaseous one. Small droplets with low speed rapidly evaporate inside the flame front, but they represent little mass and the fuel evaporation rate (Γ_F in Fig. 3(a)) stays small and does not much impact the fuel consumption rate $\dot{\omega}_F$. With $u_{rel} = 30$, the reaction zone thickness is slightly increased: droplets are large enough and move sufficiently fast to evaporate only partially within the flame thickness, as observed in Fig. 3(b). Both $\dot{\omega}_F$ and Γ_F are non-zero behind the main reaction zone, where droplets continue to evaporate. As the mixture is lean, enough oxidizer remains in the hot gas to burn the produced vapor. All droplets are finally consumed, leading to the same final burnt gas temperature T_{burnt} as the gaseous flame.

Figure 2 (b) and Figs. 4 (c) and (d) show the same profiles for case C (i.e rich mixture and moderate liquid loading) with the same relative velocities. As for case A, the spray flame temperature profile is similar to the gaseous one for $u_{rel} = 1$ and Γ_F is small compared to the fuel consumption rate $\dot{\omega}_F$. A very different behaviour is observed for $u_{rel} = 30$, where the temperature profile first reaches a maximum value, then decreases down to a burnt gas temperature that is still higher than the one of the gaseous case at the end of the computational domain. In Fig. 4(b), one can notice

that the fuel evaporation rate Γ_F is significant behind the main fuel consumption zone: a good part of the droplets cross the flame front, and evaporate in the burnt gas. However as the flame is overall rich, there is no oxidizer left in the hot gas and the fuel vapor does not burn. The effective equivalence ratio ϕ_{eff} at which the flame burns is smaller than the total equivalence ratio, and in this case closer to stoichiometry which increases the local temperature above the final burnt gas temperature. The hot gas is then cooled down by a dilution effect from the evaporating droplets which release vapor at a temperature $T_p < T_{burnt}$.

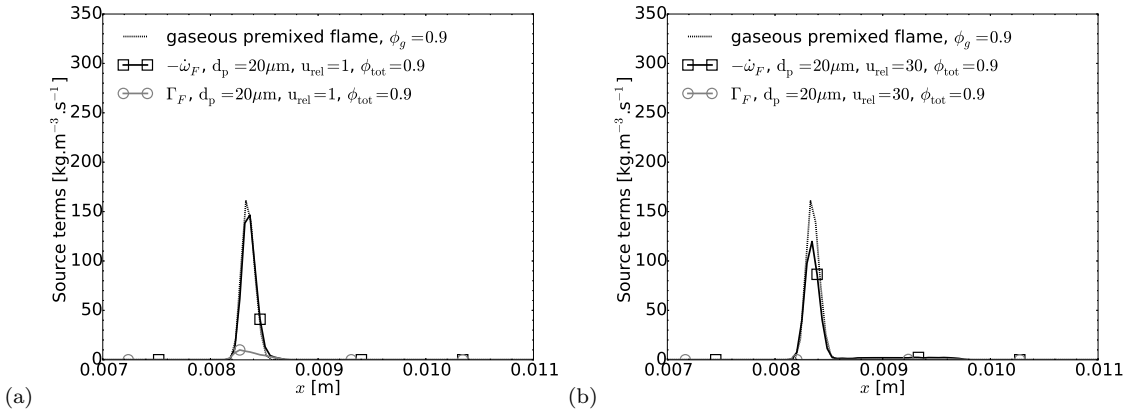

Fig. 3: *Comparison of source terms profiles for gaseous and spray flames computed with an overall equivalence ratios* $\phi_{tot} = 0.9$*:* $\phi_g = 0.8, \phi_l = 0.1$*, droplets diameter* $d_p = 20\mu m$ *and two velocity ratios (a):*$u_{rel} = 1$ *and (b):* $u_{rel} = 30$*.*

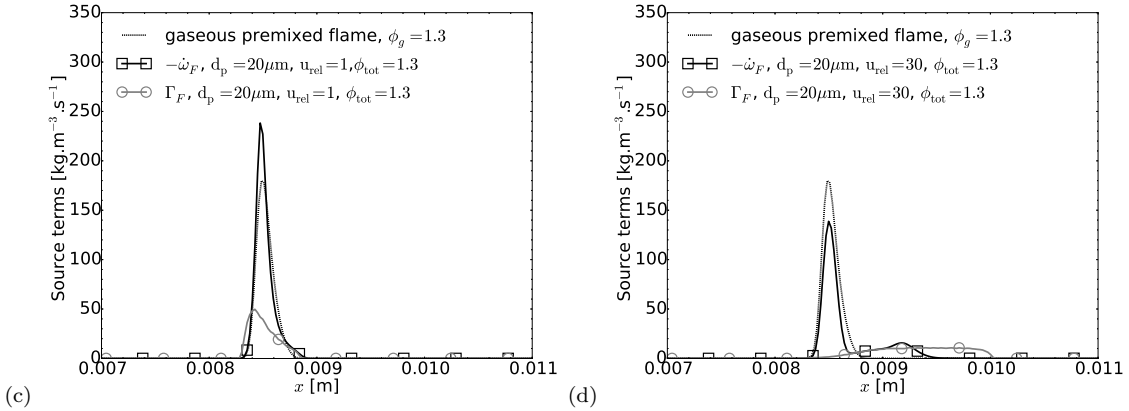

Fig. 4: *Comparison of source terms profiles for gaseous and spray flames computed with an overall equivalence ratios* $\phi_{tot} = 1.3$*:* $\phi_g = 0.8, \phi_l = 0.5$*, droplets diameter* $d_p = 20\mu m$ *and two velocity ratios (c):*$u_{rel} = 1$ *and (d):* $u_{rel} = 30$*.*

Figure 5 shows the profiles of species mass fractions for case C with the velocity ratio $u_{rel} = 30$. These profiles explain why the temperature in the hot gas remains higher than in the gaseous flame. Indeed, it can be seen that the CO-CO2 equilibrium is not reached in the hot gas, even at the end of the computational domain. In the main flame zone, CO-CO2 reached equilibrium very fast at the local equivalence ratio close to 1. In the hot gas, the equivalence ratio increases, moving the CO-CO2 equilibirum which is very long to reach then because it implies decomposition of CO2.

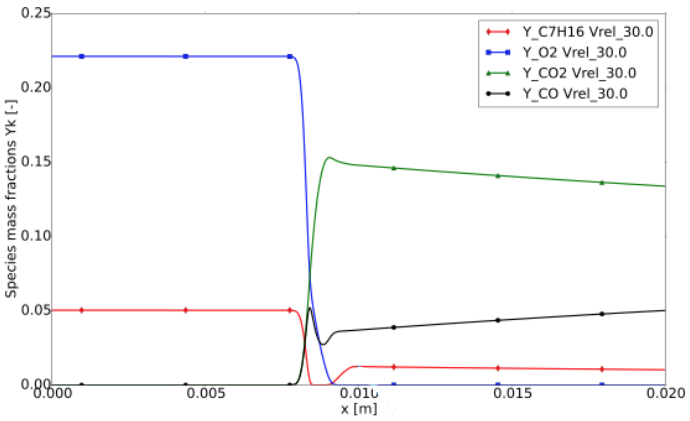

Fig. 5: *Species mass fractions profiles for the spray flame computed with an overall equivalence ratio*$\phi_{tot} = 1.3$*:* $\phi_g = 0.8, \phi_l = 0.5$*, droplets diameter* $d_p = 20\mu m$ *and a velocity raio:* $u_{rel} = 30$*.*

3.2 Two-phase laminar flame speed

The two-phase laminar flame speed S_L^{tp} is defined as the inlet fresh gas velocity required to stabilize and keep the two-phase flame steady. For all cases it has been verified that this flame speed corresponds to the flame consumption speed.

3.2.1 Lean mixture

Figure 6 shows the dependance of the two-phase laminar flame speed on droplet diameters for case A, and two velocity ratios $u_{rel} = 30$ and $u_{rel} = 1$. One can notice that S_L^{tp} never overcomes the gaseous premixed laminar flame speed. Moreover, the larger the droplets, the lower S_L^{tp} is. This behaviour is strengthened when droplets move faster than the gas.

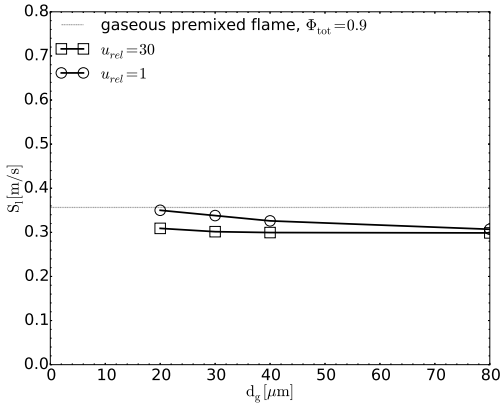

Fig. 6: *N-Heptane laminar two-phase flame speed as a function of the initial droplet diameter for an overall equivalence ratio* $\Phi_{tot} = 0.9$*, and* $\phi_g = 0.8, \phi_l = 0.1$

3.2.2 Rich mixture

Figure 7 shows the dependance of the two-phase laminar flame speed for case C. In this case S_L^{tp} may be greater than the gaseous premixed laminar flame speed. This is consistent with the higher temperature observed in Section 3.1 and has the same explanation : for rich mixtures the effective equivalence ratio ϕ_{eff} may be closer to stoichiometry than Φ_{tot}. However too high relative velocities may lead to too low ϕ_{eff}, much smaller than stoichiometry, and therefore lower flame speeds.

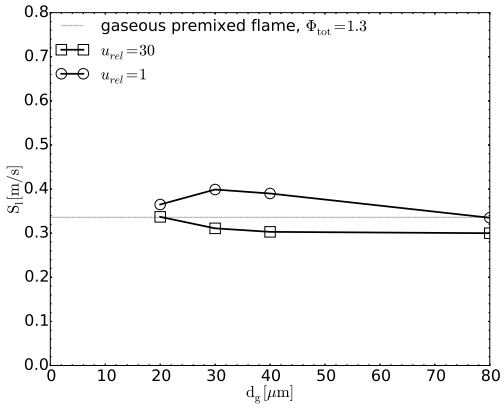

Fig. 7: *N-Heptane spray flame speed as a function of the initial droplet diameter for an overall equivalence ratio* $\Phi_{tot} = 1.3$*, and* $\phi_g = 0.8, \phi_l = 0.5$

4 Conclusions

This paper has described the effect of relative velocity between liquid and gaseous flows on a one-dimensional two-phase laminar flame. Results evidence two typical spray flame structures. The first one, identified for lean mixtures, is similar to a corresponding gaseous premixed flame in terms of burnt gas temperature profiles. In this case the relative velocity increases the flame thickness and decreases the laminar flame speed. The second one, identified for rich mixtures, is more complex. The flame burns at a lower equivalence ratio that can be closer to stoichiometry, leading to higher local gas temperature and higher flame speed than the gaseous premixed flame at the same total equivalence ratio. However if the relative velocity is too high or droplets are too large, the local equivalence ratio at which the flame burns may be very low and the two-phase flame is slower than the gaseous flame. It was also shown that the presence of droplets may significantly modify the flame chemistry, in particular in the post-flame zone. This last point should however be confirmed with more realistic chemical descriptions.

References

1. Abramzon, B., Sirignano, W.A.: Droplet vaporisation model for spray combustion calculations. Int. J. Heat and Mass Transfer **9**, 1605–1618 (1989)
2. Ballal, D.R., Lefebvre, A.H.: Flame propagation in heterogeneous mixtures of fuell droplets, fuel vapor and air. Proc. Combust. Inst. **18**, 321–327 (1981)
3. Bird, R.B., Stewart, W.E., Lighfoot, E.N.: Transport phenomena. John Wiley, New York (1960)
4. Burgoyne, J.H., Cohen, L.: The effect of drop size on flame propagation in liquid aerosols. Proceedings of the Royal Society of London A: Mathematical, Physical and Engineering Sciences **225**(1162), 375–392 (1954)
5. Dakhlia, R.F.: Combustion stationaire et instationaire de mélanges diphasiques. Phd thesis, Laboratoire d'Energétique Moléculaire et Macroscopique, Combustion (EM2C) du CNRS et de l'École Centrale de Paris (2001)
6. Franzelli, B., Riber, E., Sanjosé, M., Poinsot, T.: A two-step chemical scheme for Large-Eddy Simulation of kerosene-air flames. Combust. Flame **157**(7), 1364–1373 (2010)
7. Hayashi, S., Kumagai, S., Sakai, T.: Propagation velocity and structure of flames in droplet-vapor-air mixtures. Combust. Sci. Tech. **15**, 169–177 (1976)
8. Hirschfelder, J.O., Curtiss, F., Bird, R.B.: Molecular theory of gases and liquids. John Wiley & Sons (1964)
9. Kumar, K., Freeh, J.E., Sung, C.J., Huang, Y.: Laminar flame speeds of preheated iso-octane/o2/n2 and n-heptane/o2/n2 mixtures. Journal of Propulsion and Power **23**(2), 428–436 (2007)
10. Myers, G., Lefebvre, A.: Flame propagation in heterogeneous mixtures of fuel drops and air. Combust. Flame **66**(2), 193–210 (1986)
11. Neophytou, A., Mastorakos, E.: Simulations of laminar flame propagation in droplet mists. Combust. Flame **156**(8), 1627–1640 (2009)
12. Paulhiac, D.: Modelisation de la combustion d'un spray dans un bruleur aeronautique. Phd thesis, INP Toulouse (2010)
13. Poinsot, T., Veynante, D.: Theoretical and Numerical Combustion. Third Edition (www.cerfacs.fr/elearning) (2011)
14. Polymeropoulos, C.E.: Flame propagation in a one-dimensional liquid fuel spray. Combustion Science and Technology **9**(5-6), 197–207 (1974)
15. Schiller, L., Nauman, A.: A drag coefficient correlation. VDI Zeitung **77**, 318–320 (1935)
16. Silverman, I., Greenberg, J.B., Tambour, Y.: Stoichiometry and polydispersity effects in premixed spray flames. Combust. Flame **93**, 97–118 (1993)
17. Zhu, M., Rogg, B.: Modelling and simulation of sprays in laminar flames. Meccanica **31**, 177–193 (1996)